Received: 24 April 2023 | Revised: 26 June 2023 | Accepted: 27 June 2023

DOI: 10.1002/ijc.34665

IJC INTERNATIONAL JOURNAL of CANCER

RESEARCH ARTICLE

Innovative Tools and Methods

Multiscale quantification of morphological heterogeneity with creation of a predictor of longer survival in glioblastoma

Georg Prokop[1,2] | Benedikt Wiestler[3] | Daniel Hieber[1,4,5] | Fynn Withake[3] | Karoline Mayer[2] | Jens Gempt[6,7] | Claire Delbridge[2] | Friederike Schmidt-Graf[8] | Nicole Pfarr[2] | Bruno Märkl[1] | Jürgen Schlegel[1,2] | Friederike Liesche-Starnecker[1,2,5]

[1]Pathology, Medical Faculty, University of Augsburg, Augsburg, Germany

[2]Institute of Pathology, School of Medicine, Technical University Munich, Munich, Germany

[3]Department of Neuroradiology, Klinikum rechts der Isar, School of Medicine, Technical University Munich, Munich, Germany

[4]Institute DigiHealth, Neu-Ulm University of Applied Sciences, Neu-Ulm, Germany

[5]Bavarian Cancer Research Center (BZKF), Augsburg, Germany

[6]Department of Neurosurgery, Klinikum rechts der Isar, School of Medicine, Technical University Munich, Munich, Germany

[7]Department of Neurosurgery, University Medical Center Hamburg-Eppendorf, Hamburg, Germany

[8]Department of Neurology, Klinikum rechts der Isar, School of Medicine, Technical University Munich, Munich, Germany

Correspondence
Friederike Liesche-Starnecker, University of Augsburg, Medical Faculty, Institute of Pathology and Molecular Diagnostics, Stenglinstraße 2, 86156 Augsburg, Germany.
Email: friederike.liesche-starnecker@uka-science.de

Funding information
Bavarian Cancer Research Center (BZKF), Grant/Award Number: ZB-003-2022; Deutsche Forschungsgemeinschaft (subproject B12), Grant/Award Number: SFB 824

Abstract

Intratumor heterogeneity is a main cause of the dismal prognosis of glioblastoma (GBM). Yet, there remains a lack of a uniform assessment of the degree of heterogeneity. With a multiscale approach, we addressed the hypothesis that intratumor heterogeneity exists on different levels comprising traditional regional analyses, but also innovative methods including computer-assisted analysis of tumor morphology combined with epigenomic data. With this aim, 157 biopsies of 37 patients with therapy-naive IDH-wildtype GBM were analyzed regarding the intratumor variance of protein expression of glial marker GFAP, microglia marker Iba1 and proliferation marker Mib1. Hematoxylin and eosin stained slides were evaluated for tumor vascularization. For the estimation of pixel intensity and nuclear profiling, automated analysis was used. Additionally, DNA methylation profiling was conducted separately for the single biopsies. Scoring systems were established to integrate several parameters into one score for the four examined modalities of heterogeneity (regional, cellular, pixel-level and epigenomic). As a result, we could show that heterogeneity was detected in all four modalities. Furthermore, for the regional, cellular and epigenomic level, we confirmed the results of earlier studies stating that a higher degree of heterogeneity is associated with poorer overall survival. To integrate all modalities into one score, we designed a predictor of longer survival, which showed a highly significant separation regarding the OS. In conclusion, multiscale intratumor heterogeneity exists in glioblastoma and its degree has an impact on overall survival. In future studies, the implementation of a broadly feasible heterogeneity index should be considered.

KEYWORDS
automated analysis, brain tumor, glioblastoma, heterogeneity, methylation, morphology

Abbreviations: FFPE, formalin-fixation and paraffin-embedded; GBM, glioblastoma; GBM_3+, cohort with a minimum of three biopsies with methylation class "glioblastoma"; GFAP, glial fibrillary acidic protein; HE, hematoxylin and eosin; HisScore, histology score; Iba1, ionized calcium binding protein 1; IHC, immunohistochemical/immunohistochemistry; IRS, immunoreactive score; lv, level; MAD, median absolute deviation; MGMT, *O*-6-methylguanin-DNA-methyltransferase; Mib1, molecular immunology borstel 1; NucDivScore, nuclear diversity score; OS, overall survival; PCA, principial component analysis; ProLoS, predictor of longer survival; RTK-1, receptor tyrosine kinase-I; t-SNE, t-distributed stochastic neighbor embedding; TUM, Technical University of Munich; UniPreHet, unified prediction of heterogeneity.

[Correction added on 11 August 2023, after first online publication: There were errors in the order of author affiliations and have been updated in this version.]

What's new?

Overall survival of glioblastoma patients may be influenced by intratumor heterogeneity, although standard procedures to quantify heterogeneity in histological preparations are lacking. In our study, the authors developed scoring systems for the assessment of heterogeneity in glioblastoma based on differences in regional protein expression, nuclear features in cells, pixel intensity within tumors and epigenomic methylation. Heterogeneity was detected at all levels, with an elevated degree of heterogeneity associated with reduced overall survival. Degree of heterogeneity was correlated with biopsy distance at regional and epigenetic levels. The findings highlight the potential utility of a heterogeneity index for prognostic evaluation in glioblastoma.

1 | INTRODUCTION

Intratumor heterogeneity is a hallmark of glioblastoma (GBM)[1] and possibly at the root of its dismal prognosis and therapy resistance. Beside a pronounced morphological variety, the heterogeneity includes genomic and epigenomic aberrations.[2] Based on the work by Verhaak et al,[3] many efforts to define glioblastoma subtypes have been made, especially after it was shown that different GBM subtypes have diverse clinical outcomes.[4] Most studies were based on analyses of high-resolution data, including genomic and epigenomic tumor information. These "omic"-approaches give detailed, comprehensive insights into the tumor's molecular characteristics, but have the disadvantage to neglect the tumor's morphology, including intratumor heterogeneity. Cellular diversity is essential for malignant neoplasia as GBM, though, because it allows the tumor to adapt and survive harsh microenvironments or cytotoxic anticancer therapeutics including radiation and temozolomide.[5] This is why recent studies have focused on spatial heterogeneity within one tumor using morphological or molecular approaches including single-cell sequencing or methylation analysis.[6-9]

In previous studies, our study group has focused on the morphological itemization of intratumor heterogeneity in GBM. After defining areas of interest with respect to different morphology and protein expression, methylation profiling confirmed that our spatial separation was valid and is of relevance, since areas of the same tumor showed varying methylation profiles.[7] This result was corroborated by a prospective study that analyzed the methylome of 238 biopsies of 56 GBM patients showing that 39% of the tumors were composed of different subtypes.[10] Other groups with a similar approach proved a varying GBM subclass assignation between spatially distant samples of individual tumors.[9,11] Moreover, we proved that the degree of heterogeneity has prognostic impact.[7]

The samples generated through the prospective study of Gempt et al[10] are of high value regarding their exceptional spatial separation, which offers the chance for comprehensive morphological characterization of intratumor heterogeneity. With a multiscale approach, we analyzed these samples to address the hypothesis that intratumor heterogeneity exists on different levels (Figure 1A) comprising traditional regional analyses based on hematoxylin and eosin (HE) and immunohistochemical (IHC) stains, but also innovative methods including computer-assisted analysis of tumor cell nuclei shape and pixel intensities combined with epigenomic data of the tumor areas. Heterogeneity on the regional and cellular level was quantified by utilizing preexisting scoring systems and aided by the established CellProfiler software.[12] We characterized the methylation profile using the brain tumor classifier based on the work by Capper et al.[13] The Simpson and Shannon Diversity Index, both originally used to describe ecological diversity, served as markers for the variability of pixel intensities. To prove the clinical relevance of our study, we designed a predictor of longer survival which integrates all four defined levels.

2 | MATERIALS AND METHODS

2.1 | Material

The tissue samples of 197 biopsies of 49 patients with therapy-naive IDH-wildtype glioblastoma which derived from a cohort of a prospective study[10] were included. For that study, 2 to 9 biopsies of each tumor were retrieved prior to tumor resection. All surgeries including biopsy retrieval were performed at the Department of Neurosurgery of the Klinikum rechts der Isar, Technical University of Munich (TUM) between February 2018 and March 2021. Inclusion criterion for the present study was a minimum of three evaluable biopsies per patient (Figure 1B); 42/48 patients met this inclusion criterion. During evaluation, several slides were excluded for following reasons: not enough material of tumor core left for histopathological analysis (exclusion of 17 slides) or predominantly necrotic material (exclusion of 3 slides). Due to slide exclusion, all samples of five patients were eliminated because the number of evaluable biopsies dropped under 3.

The final cohort included 157 biopsies of 37 patients (median age at diagnosis 69.1 years; 23 male; Table 1). All tumors were reevaluated and classified according to the fifth version of the WHO classification of brain tumors from 2021[14] for the present study. The promotor of the *O*-6-methylguanin-DNA-methyltransferase (MGMT) was methylated in 14 (38%) patients. The amount of biopsies per patient ranged from 3 to 7 (median 4). For 28 patients, DNA methylation profiling was performed for a minimum of three biopsies, leading to evaluable methylation data of 108 samples.

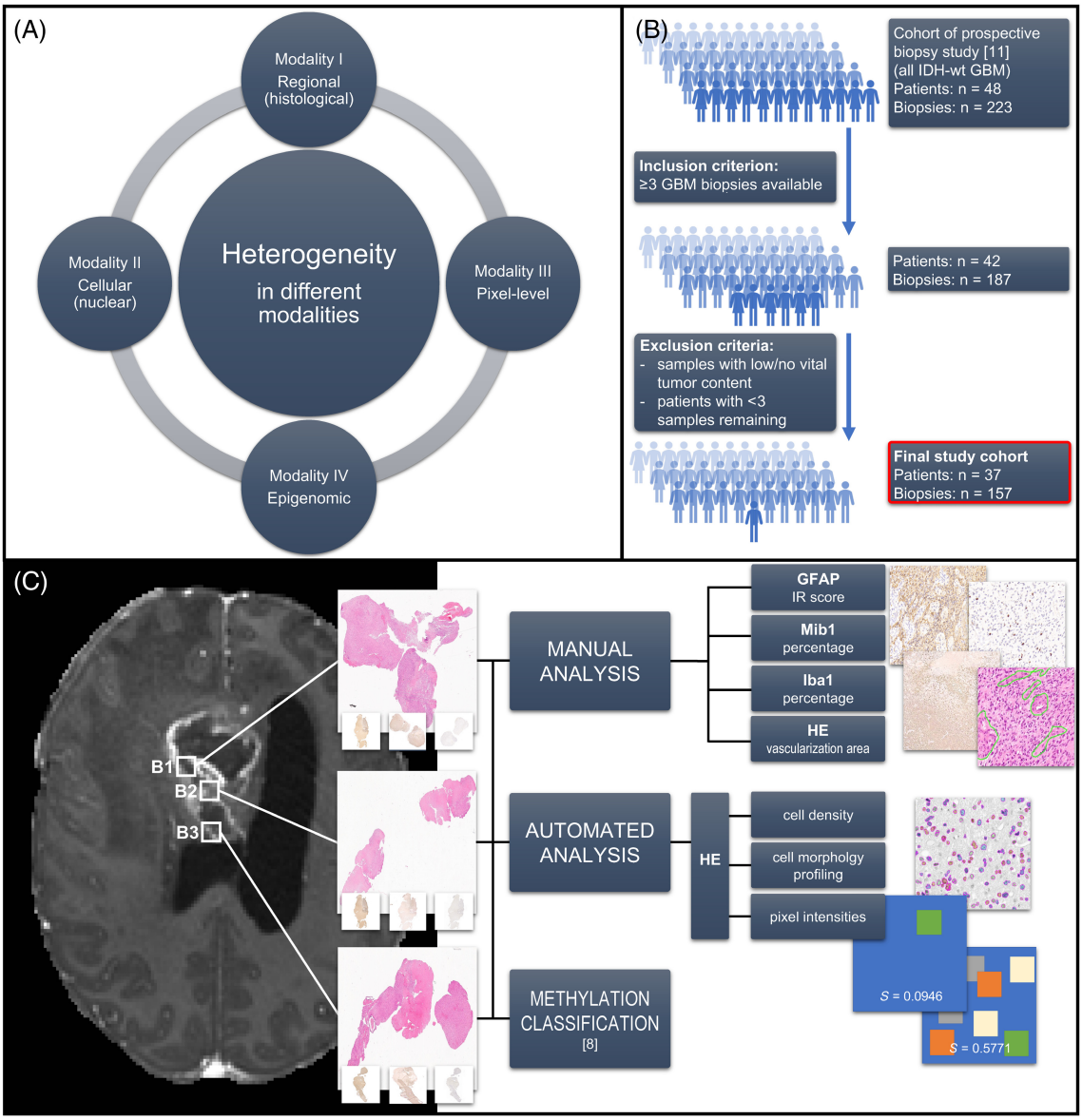

FIGURE 1 Study concept and workflow. (A) visualizes the principal concept of our study with the four levels of heterogeneity. In (B), a flow chart gives information about initial and final study cohort, as well as the inclusion and exclusion criteria. The principal workflow is depicted in (C).

2.2 | Methods

2.2.1 | Workflow

The project design is shown schematically in Figure 1C.

2.2.2 | Hematoxylin and eosin staining and immunohistochemistry

HE staining was performed following standard protocol. For immunohistochemistry, 2 µm thick slides were dried at room temperature for 30 minutes. After epitope uncovering in pH 6.0 citrate buffer at 95°C for 30 minutes and H_2O_2 incubation, the slides were charged with the primary antibodies (anti-GFAP: monoclonal, mouse, dilution 1:400; Clone 6F2; DakoCytomation Denmark A/S, Denmark; anti-Iba1: polyclonal, rabbit, dilution 1:500; Wako Pure Chemical Industries, Japan; anti-Ki-67 (Mib-1): monoclonal, rabbit, dilution 1:200; Clone SP6; Thermo Fisher Scientific, Waltham, MA) overnight at 4°C. Biotinylated secondary anti-mouse for GFAP and Mib1 and anti-rabbit for Iba1 IgG (Vector Laboratories, Burlingame, CA) all in a dilution of 1:400, followed by ABC reagent (Vector Laboratories, Burlingame, CA) were incubated for 30 minutes each. Subsequently, DAB reagent was added. For all immunostainings, counterstaining with hematoxylin was conducted.

TABLE 1 Patient data.

	Complete cohort	Cohort with DNA methylation profiling of ≥3 samples
Number of patients	37	28
Number of biopsies		
Total	157	108
Per patient median	4	4
Per patient range	3-7	3-6
Age at diagnosis (years)		
Median	69.1	67.9
Mean	66.7	66.9
Range	34-87	34-87
Sex		
Male	23 (62%)	17 (61%)
Female	14 (38%)	11 (39%)
MGMT promotor status		
Methylated	14 (38%)	12 (43%)
Nonmethylated	23 (62%)	16 (57%)
Registered cases of death	20 (53%)	16 (57%)
Registered cases with relapse	17 (46%)	12 (43%)

2.2.3 | Manual staining evaluation

GFAP immunohistochemistry was evaluated using the established semi-quantitative immunoreactive score (IRS) by Remmele and Stegner, which is a product of scores for staining intensity (0 = no staining, 1 = weak, 2 = moderate, 3 = strong positivity) and percentage of immunoreactive cells (0 = 0%, 1 = 1%-4%, 2 = 5%-50%, 3 = 51%-75%, 4 = 76%-100%).[15] For Iba1 and Mib1, a percentage of positive cells in all vital cells was assigned for every biopsy. The manual staining evaluation was performed by one experienced neuropathologist. The vasculature was assessed by digitally measuring the size of the tumor tissue and the area consisting of vessels within by outlining vessel structures. The proportional area covered by vessels was used for further analysis.

2.2.4 | Histopathological image acquisition

For the automated image analysis, all slides were digitized using the Aperio AT2 scanner (Leica biosystems, Wetzlar, Germany). To avoid confounding by varying tumor size and content, two different snapshots of the core tumor region of each biopsy were taken, resulting in a total of 314 images. To ensure a fixed size, each image was cropped to 750 by 750 µm (1272 × 1272 pixels) during the following processing steps.

2.2.5 | CellProfiler analysis and clustering

The software CellProfiler[12] was used to detect the nuclei and extract nuclear features from the images. The detection was performed using the 3-threshold Otsu filter. Exactly 154 features of the modules MeasureObjectSizeShape, MeasureObjectIntensity, MeasureImageQuality, MeasureTexture, MeasureImageAreaOcupied and MeasureImageIntensity were extracted. To assess the nuclear heterogeneity, we normalized the features according to the manufactures standards and calculated the nuclear diversity score as described previously from the features median radius, mean and median intensity per nucleus.[16]

For cluster analysis of nuclear features, we excluded five features with nonchanging values (NucObj_Children_RelabeledNuclei_Count, NucObj_AreaShape_EulerNumber, NucObj_Location_Center_Z, NucObj_Location_MaxIntensity_Z_OrigGray, NucObj_Location_CenterMass Intensity_Z_OrigGray) and two counting variables (NucObj_Number_Object_Number, ObjectNumber). Afterwards, *z*-scale normalization and feature selection based on pairwise correlation resulting in four datasets (*z*-scaled and original dataset, with or without feature selection [cut-off set at 0.95]) was performed as suggested previously.[17]

2.2.6 | Quantification of pixel intensities

Custom made Python scripts (Python version 3.9.5) were used to quantify the information content of pixel intensities in the aforementioned snapshots (see Materials and Methods in Data S1). To do so, firstly, the images were converted into greyscale images, followed by calculating the distribution of pixel intensities as a histogram consisting of either 25, 50 or 256 bars. After filtering intensities with the frequency of 0, the Simpson and Shannon Diversity index were calculated as follows[18,19]:

Simpson index:

$$D = 1 - \sum_{i=1}^{S} p_i^2$$

Shannon-diversity index:

$$H' = -\sum_{i=1}^{S} p_i \times \ln p_i$$

S is the total number of groups of pixel intensities and *p* the proportion of the individual pixel intensity group.

2.2.7 | 850k methylation array

DNA was extracted from the formalin-fixed and paraffin-embedded (FFPE) material of the total biopsies. After measuring the DNA concentration using the Quibits dsDNA High sensitivity Assay kit (Invitrogen, Waltham, MA) on a QuBit 4 system, the DNA was applied to an Illumina EPIC BeadChip (Illumina, San Diego, CA) for methylation analysis as previously described.[20] For tumor classification, the brain tumor classifier based on the work by Capper et al[21] and available at the platform https://www.molecularneuropathology.org/ in version v12.3 was used.

For each sample, the prediction with the highest methylation class score was regarded the "main methylation class." Classes titled "Glioblastoma …" were considered as GBM-related diagnosis.

2.2.8 | Scoring systems

During analysis, several scoring systems have been used to simplify the concept of heterogeneity.

Histology score (HisScore)

The *HisScore* synergizes all regional parameters (IHC stains plus HE assessment of the area of vasculature) into one single number devised as following: For each parameter p was determined whether the SD (SD) in tumor t is greater than the median SD across all tumors T. A score of 1 for parameters above the median and a score of 0 for parameters below or equal to the median SD was assigned. Summing up these scoring points resulted in the *HisScore* (Figure 2A).

$$HisScore_t = \sum(P_t), \text{where } P : = (score_{Iba}, score_{GFAP}, score_{Mib}, score_{Vasc.\ Area})$$

$$\text{with } score_x = 1 \text{ if } (SD(p_t) > SD(p_T))$$

$$\text{and } score_x = 0 \text{ if } (SD(p_t) \leq SD(p_T)).$$

2.2.9 | Nuclear diversity score (*NucDivScore*)

In the HE images, cell nuclei were detected and measured using the CellProfiler software.[12]

For each nucleus, size (reproduced as mean radius) and staining intensity (reproduced as median and mean intensity) was estimated and the *NucDivScore* generated as described previously.[16] For each image I, nuclear diversity d was quantified from the variability of morphological features f, measured for nuclei in that image.

$$d_f^I = \text{MAD}_{\text{Nuclei}}(f), \text{where } f : = \{\text{mean radius}, \text{median intensity}, \text{mean intensity}\}.$$

Nuclear diversity for each tumor t was then calculated as the median normalized nuclear diversity across all images from that tumor:

$$d_f^t = \text{Median}_{I \in t}\left(d_t^I\right).$$

Nuclear diversity ranks R_f^t were calculated for each tumor by sorting tumor samples according to the corresponding diversity feature. The final quantification of the nuclear diversity score (D^t) for each tumor t was derived from the median diversity rank (Figure 2D):

$$D^t = \frac{\text{Median}_f\left(R_f^t\right)}{\max\left(\text{Median}_f\left(R_f^t\right)\right)}$$

2.2.10 | Entity ratio

The *entity ratio* is used to assess heterogeneity on the epigenetic level. After excluding all biopsies with non-GBM methylation classes as predicted by the brain tumor classifier based on the work by Capper et al,[21] the ratio is determined only for patients with a minimum of three remaining biopsies. The ratio is then calculated by dividing the number of different GBM-related methylation classes found in one tumor by the number of included samples per tumor as following:

$$\text{Entity ratio}_t = \frac{(\text{number of different GBM entities})_t}{(\text{number of analyzed samples})_t}$$

2.2.11 | Unified prediction of heterogeneity (*UniPreHet*)-Ratio

The *UniPreHet-Ratio* is used to incorporate all heterogeneity predictions into a single score. It consists of the number of heterogenous levels per tumor t divided by the number of contributing levels.

$$\text{UniPreHet} - \text{Ratio}_t = \frac{\Sigma(\text{heterogenous levels})_t}{\Sigma(\text{contributing levels})_t}$$

A level is heterogenous, if parameter x of tumor t is greater than the median of x across all tumors T.

$$x_t > \text{median}(x_T)$$

2.2.12 | Predictor of longer survival (*ProLoS*)

The *ProLoS* is a ratio that reflects the impact on survival for each level. First, it is determined whether the tumor's induvial value v of *HisScore*, *NucDivScore* and *Entity Ratio* is higher than the median of v across all tumors T.

$$Score_{HisScore,NucDivScore,Entity\ Ratio} = 1 \text{ if } ((v_t) > \text{median}(v_T))$$

$$Score_{HisScore,NucDivScore,Entity\ Ratio} = 0 \text{ if } ((v_t) \leq \text{median}(v_T))$$

For the pixel-level, a score of 1 is awarded when v is smaller than the median.

$$Score_{pictorial} = 1 \text{ if } ((v_t) < \text{median}(v_T))$$

$$Score_{pictorial} = 0 \text{ if } ((t) \geq \text{median}(v_T))$$

The final *ProLoS* consists of the sum of all levels divided by the number of levels.

$$ProLoS_t = \frac{\Sigma(\text{scoring points})_t}{\Sigma(\text{contributing levels})_t}.$$

2.2.13 | Statistical analysis

All statistical analyses were performed using R (version 4.0.2). Survival analyses were performed using the survival[22] and survminer package. Kaplan-Meier curves were compared using the log-rank test. The t-distributed stochastic neighbor embedding (t-SNE) clustering,[23]

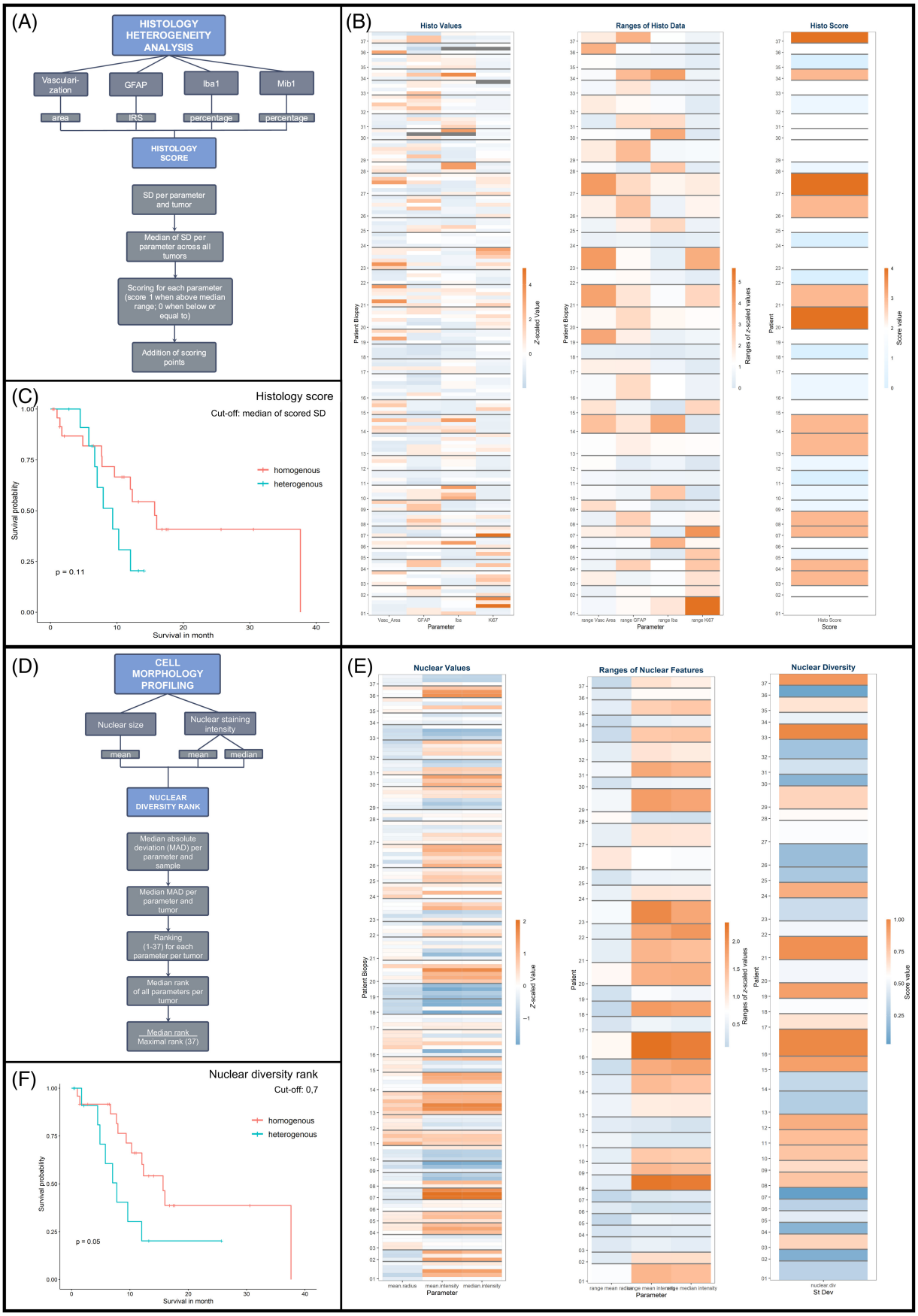

FIGURE 2 Legend on next page.

k-means cluster analysis and principial component analysis (PCA) were performed on the dataset of nucleus features. Correlations were tested using Pearson's method or Spearman's method. Hazard ratios were calculated using Cox proportional hazard regression model. For all tests, statistical significance was defined as $P < .05$.

3 | RESULTS

3.1 | Heterogeneity is present in all modalities and shows association with overall survival

In this part, it is shown that heterogeneity exists in all four modalities and that each heterogeneity has an impact on the overall survival (OS). For every modality, we have defined indices of heterogeneity that mostly apply the standard deviations (SD) as values of variance. For the histological/regional parameters and the nuclear profiling, scores were used to integrate the different parameters into one value.

3.1.1 | Modality I: Regional (histological) level

Regional heterogeneity expressed as differences in expression levels of proteins is ubiquitous. To quantify heterogeneity and to integrate all parameters of the regional level, we used the *HisScore* (Figure 2A). Groups of heterogenous and homogenous tumors were built by separating them with regard to the median *HisScore* (above median [=2] equates to heterogenous; below or equal to homogenous). By doing so, 12 tumors were assigned to the heterogenous group, while 25 tumors were homogenous. Strikingly, a clear statement about the association of heterogenous or homogenous phenotype with the OS can be made. Although not significant, patients with heterogenous tumors showed a poorer OS compared to patients with tumors of the homogenous group (median survival of 9.36 months vs 15.67 months; $P = .108$; Figure 2B).

The single parameters were also isolatedly examined. We assessed range and SD as values of heterogeneity. The maximal values observed are listed in Table S1. To visualize the intratumor heterogeneity, the values of all parameters and samples were normalized using the z-transformation. Thus, it is depicted how many standard deviations each value deviates from the overall mean value (a high z-score value equals a high measured value). Figure 2C depicts the corresponding false color image of the values of each biopsy sorted by patient. Apparently, the values are not distributed equally and have a rather high range from −1.975 to 4.068. As can be seen in patient 14, both high and low histological values can occur in one tumor indicating high histological heterogeneity (range of *z*-score values for patient 14: GFAP 1.982, Iba 3.858, Mib1 0.0830, Vasc_Area 3.121). However, when considering patient 18, a clear visualization of a histological homogenous tumor with only low maximal ranges of the *z*-score values can be observed (GFAP 0.330, Iba1 0.193, Mib1 0.415, Vasc_Area 0.407).

Furthermore, the single parameters were correlated with each other (Table 2). As to be expected, a significant negative correlation is seen between Iba1-positive cells and Mib1 ($r = -.233$; $P = .004$). No further significant correlation is observed. When examining an association between OS and the single parameters, no clearly identifiable separation between tumors with high parameter ranges and tumors with homogenously distributed parameters is observed (data not shown).

3.1.2 | Modality II: Cellular (nuclear) level

Heterogeneity on the cellular level includes differences in nuclear form, size and staining intensity. In the HE images, cell nuclei were detected and measured using the CellProfiler software.[12] The different parameters were then integrated into one *NucDivScore* (Figure 2D). Afterwards, the tumors were divided into heterogenous and homogenous tumors by separating them with regard to the median *NucDivScore* (above median [=0.54285] equates to heterogenous; below or equal to homogenous). Seventeen tumors were assigned to the heterogenous group, while 20 tumors were homogenous.

Also in this modality, a distinct, although not significant separation with shorter OS for heterogenous tumors (median survival of 9.63 months compared to 12.32 months; $P = .170$; data not shown) is seen. When the cut-off is set to 0.7 instead of the median, a significant separation can be seen (median survival of 7.75 months for heterogenous tumors compared to 15.67 months for homogenous tumors; $P = .0498$; Figure 2E). In this case, 13 tumors were assigned to the heterogenous group, 24 to the homogenous group.

To visualize the heterogeneity of the single parameters, the values of all parameters and samples were again, translated into *z*-score values (Figure 2F). The tumor of patient 16 is an example for a heterogenous tumor regarding the diversity of the nuclear shape (range of *z*-score values: mean radius 0.820, mean intensity 2.345, median intensity 2.206). In contrast, the tumor of patient 6 is

FIGURE 2 Modalities I and II: Regional and cellular level. (A) demonstrates schematically the built-up of the *HisScore*. In (B), a distinct, although not significant, separation with poorer OS of patients with tumors that are heterogenous regarding their *HisScore* is seen, when dividing two groups by the median *HisScore*. Part figure (C) shows the *z*-scaled values (left) and the ranges of those *z*-scaled values of the single histological parameters vascularization area, GFAP, Iba1 and Mib1 expression, as well as the integrating *HisScores* (right) for every patient. Part figure (D) demonstrates schematically the built-up of the *NucDivScore*. In (E), a distinct separation with poorer OS of patients with tumors that are heterogenous regarding their *NucDivScore* is seen, when dividing two groups by a cut-off of 0.7. Part figure (F) shows the *z*-scaled values (left) and the ranges of those *z*-scaled values (middle) of the single cellular/nuclear parameters mean radius, mean intensity and median intensity, as well as the integrating *NucDivScore* (right) for every patient.

TABLE 2 Correlation of histological parameters.

Parameter		Vasc_Area	GFAP	Iba1	Mib1
Vasc_Area	*r*		.126	.047	.096
	P		.281	.562	.237
GFAP	*r*	.126		.097	−.087
	P	.281		.228	.281
Iba1	*r*	.047	.097		−.233
	P	.562	.228		.003
Mib1	*r*	.096	−.087	−.233	
	P	.237	.281	.003	

homogenous in the nuclear parameters (range of *z*-score values: mean radius 0.390, mean intensity 0.221, median intensity 0.209).

Additionally, we investigated whether a separation of different nuclei types based on shape, intensity and texture features of the nuclei extracted by CellProfiler software could be achieved. For this, we tested the original data, a *z*-scaled dataset both with and without feature selection based on pairwise correlation. A principial component, k-means- and t-SNE cluster analysis was performed on the four resulting datasets. However, no meaningful separation could be achieved in all (data not shown).

3.1.3 | Modality III: Pixel-level

GBM show diverging visual facets. To quantify heterogeneity on the pixel-level, we measured the diversity of pixel intensities in the 314 HE images (ranging from 6 to 14 images per patient depending on the number of biopsies) using the Shannon and Simpson Diversity Indices. Figure 3A displays an example of a histogram of the pixel distribution.

Overall, we observed rather high values in the calculated indices (Table S2) indicating high information content or rather high diversity in pixel intensities. As to be expected, all the single parameters correlate strongly and significantly with each other (data not shown).

To visualize the heterogeneity of the parameters of the pixel-level, the values of all parameters and samples were, again, translated into *z*-score values (Figure 3B). Patient 23 shows a heterogenous tumor regarding the pixel diversity values (range of *z*-score values: Simpson-256 3.757, Shannon-256 4.162). In contrast, the tumor of patient 22 is more homogenous (range of *z*-score values: Simpson-256 2.773, Shannon-256 2.569).

To integrate all samples into a single parameter, the median and the SD of each index across all samples of a tumor was calculated. Again, we divided the tumors into heterogenous and homogenous tumors by separating them with regard to the median (above median equating to heterogenous; below or equal to homogenous). When observing the median of a patient's Simpson or Shannon Diversity Index, no clear trend in the survival was observed (data not shown). However, when quantifying the pixel information as the SD of the Simpson Diversity Index of all sample images from a patient (with a histogram with 256 bars), a significant shorter survival is seen for the homogenous tumors (9.63 months compared to 37.62 months; $P = .016$; cut-off median of 0.00246; Figure 3C) with 18 tumors assigned to the heterogenous group and 19 tumors assigned to the homogenous group. Thus, interestingly, the results of the pixel analyses show a diverging direction to the other levels.

3.1.4 | Modality IV: Epigenetic level

To assess epigenomic heterogeneity, we used a 850k methylation array and classified the results using the brain tumor classifier based on the work by Capper et al[21] in version v12.3. In total, 140 samples were classified resulting in 17 different main methylation classes ("all_samples"), of which 137 were tumor-related diagnoses. Exactly 117 samples had a GBM-related diagnosis with seven different subclasses. Three biopsies were classified as control class. See Figure 3D for complete classifier assignments.

For further analyses, non-GBM diagnoses were excluded to prevent deceptive results due to sampling error or DNA quality defect. To assess the heterogeneity, only patients with a minimum of 3 biopsies with GBM diagnosis were included ("GBM_3+") resulting in a collective of 108 biopsies of 28 tumors).

The biopsies of five tumors (17.9%) were assigned to three different methylation classes. Nine tumors (32.1%) had samples with two different classes, 14 tumors (50%) with one.

For association analysis between variation of methylation classes and survival, an *entity ratio* comprised of the number of different methylation classes found in one tumor divided by the number of analyzed samples per tumor was generated. By dividing two groups by means of the median of 0.367 (above median equates to heterogenous; below or equal to homogenous), an obvious, although not significant shorter OS is observed for patients with heterogenous tumors (15.67 months vs 7.95 months; $P = .070$; data not shown). When separating by the number of different methylation classes (ranging from 1 to 3), the shortest OS is seen for tumors with three different methylation classes, whereas tumors of which all samples were classified in the same class, have the longest OS (5.78 vs 15.67 months; 10.97 months for tumor with two different classes; Figure 3E). The survival difference of tumors with only one methylation class and tumors with three methylation classes is highly significant ($P = .0046$).

3.2 | The association of different levels of heterogeneity among each other

After confirming that intratumor heterogeneity exists in our cohort, the next step was to evaluate if the different modalities of heterogeneity coexist or if one modality dominates in the individual patients. For this analysis, we chose the most comprehensive and representative parameter (complex) for each modality.

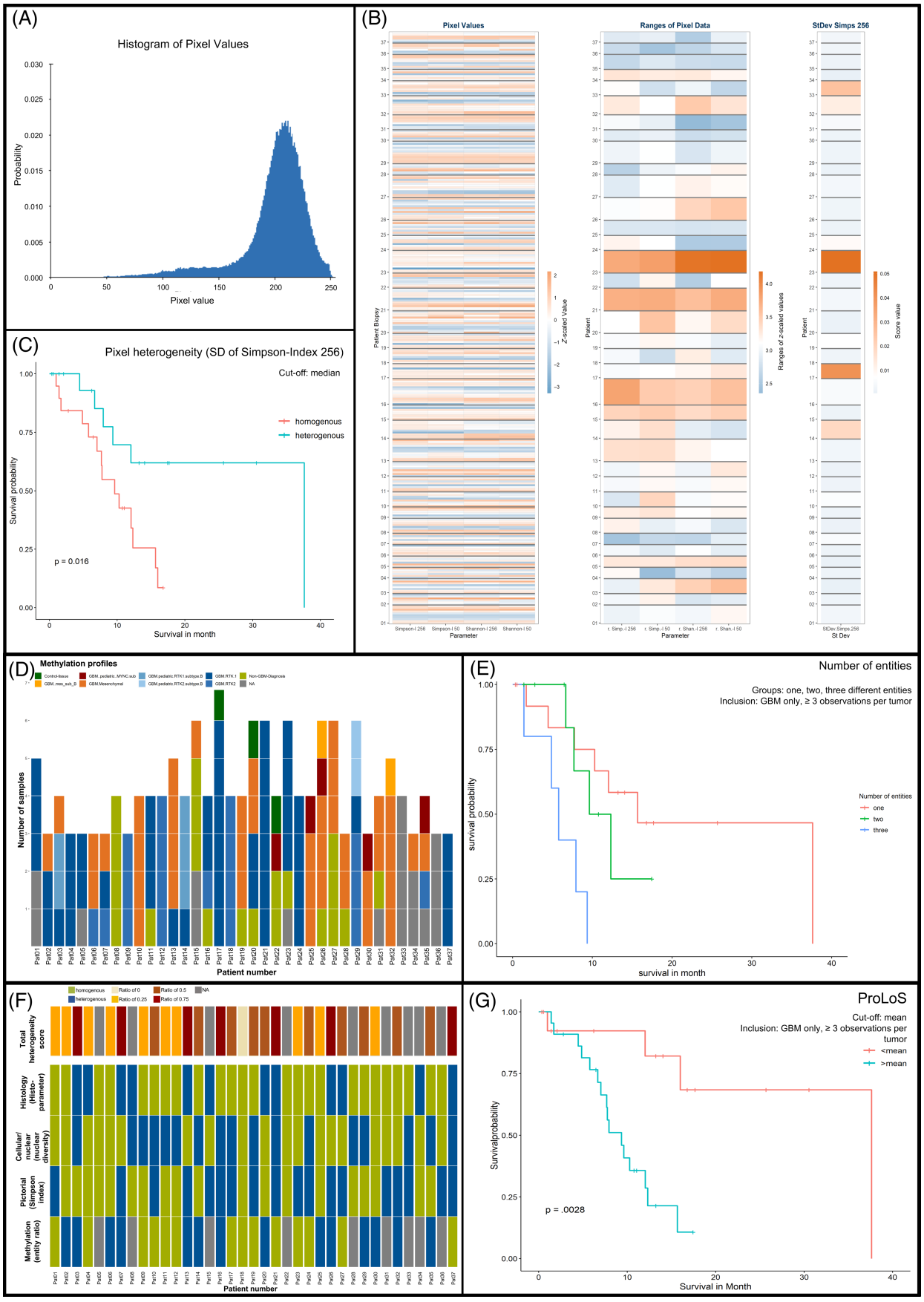

FIGURE 3 Legend on next page.

We used the *HisScore* for the regional, the *NucDivScore* for the cellular (nuclear), the SD of the Simpson Index for the pixel-level modality and the *entity ratio* for epigenetic heterogeneity.

For every patient, we determined whether each parameter was above the median leading to the assignment of a heterogeneous type. In case the parameter was below or equal to the median, a homogenous type was assumed.

Regarding the epigenomic heterogeneity, only GBM_3+ tumors were included. Three (8.1%) tumors were homogenous on all available levels (for two tumor methylation profiling and therefore, entity ratio was not available; Figure 3F). Exactly 14 (37.8%) tumors had one parameter (4 tumors without methylation profiling), 13 (35.1%) tumors had two parameters with heterogenous character (3 tumor without methylation profiling). For 7 (18.9%) tumors, three parameters were of heterogenous layout. No tumor was heterogenous in all four modalities.

Correlation analyses between the parameters of the different modalities revealed a significant correlation between the *entity ratio* and *NucDicScore* ($r = -.542$, $P = .003$). Furthermore, the *entity ratio* and SD of the Simpson Diversity Index were negatively associated, not significantly, though ($r = -.345$, $P = .072$).

The mesenchymal GBM subtype as determined by the brain tumor classifier, was significantly positively correlated with the IHC scores of Iba1 ($r = .372$, $P = .00004$) and GFAP ($r = .226$, $P = .015$). There was a negative association with the amount of Mib1-positive cells ($r = -.234$, $P = .011$). The receptor tyrosine kinase-I (RTK-I) subtype showed a significant positive correlation with Mib1 ($r = .252$, $P = .006$) and a negative correlation with Iba1-positive cells ($r = -.201$, $P = .031$). For these correlation analyses, all samples with methylation class "glioblastoma" were included.

3.3 | Creation of a predictor of longer survival integrating all levels of heterogeneity

For the analysis of the association between number of heterogenous modalities and survival, we divided the number of heterogenous levels by the number of available levels to avoid bias by missing data from modalities resulting in the *UniPreHet-Ratio*. Once again, we used the median of all *UniPreHet-Ratios* as cut-off. When considering all available data from all modalities, no clear trend was observed. However, when only taking the regional, nuclear and epigenomic modalities into account (thus, discarding the pixel-level modality), a trend toward longer survival in homogenous patients was seen (median survival 12.32 month vs 9.36; $P = .342$). This trend is even more apparent, when only samples with GBM as main classifier diagnosis served as basis for the entity ratio. While the survival difference for all modalities is not significant (median survival 12.32 vs 7.95 months; $P = .237$), a significant survival difference can be seen in the reduced *UniPreHet-Ratio* (without pixel-level; median survival 16.00 vs 7.95 months; $P = .0496$).

We further tested whether the four modalities could form a sufficient predictor of longer survival (*ProLoS*). To this end, the *HisScore*, the *NucDivScore* and the *entity ratio* were weighted analogously to the *UniPreHet-Ratio*. For the pixel-level heterogeneity, however, a score point was assigned when the value was below or equal to the median reflecting its association with patient survival. Again, the scores of all modalities were added and divided by the number of contributing modalities to avoid bias by missing data. To test the survival, we split the patients in two groups based on the median of the overall ProLoS. While splitting by the median (median(*ProLoS*) = 0.5) results in a clear, yet nonsignificant trend (median OS 12.32 vs 7.03 month; $P = .117$), it splits the cohort unevenly (*ProLoS* > median is true for only 6 patients and false for 31). Therefore, we additionally tested the mean (mean(*ProLoS*) = 0.421) as a cut-off resulting in a more even separation (*ProLoS* > mean is true for 15 and false for 22 patients) and a significant split regarding the OS (median OS 37.62 vs 9.36 month; $P = .002$). This holds also true with a GBM_3+ precondition as basis for the entity ratio (median survival 37.62 vs 9.36 month; $P = .003$; Figure 3G).

Additionally, we built a cox hazard model to examine the different impact of the parameters on the *ProLoS*. While all parameters of the *ProLoS* seem to be associated with longer survival, only the regional and the pixel-level show a significant association (regional $P = .03$, pixel-level $P = .016$ | for gbm 3+: regional $P = .023$, pixel-level $P = .026$, cellular: $P = .05$).

3.4 | Correlation analysis between tumor size and biopsy distances with degree of heterogeneity

In a last step, we assessed a possible correlation between tumor size and distances of the biopsies with the degree of heterogeneity. Information on tumor size was available for 35 patients, biopsy distance

FIGURE 3 Modalities III and IV—Pixel-level and epigenetic level—and integration of all four modalities. Part figure (A) demonstrates an example for the distribution of pixel values. In (B), a significant separation with poorer OS of patients with tumors that are homogenous regarding their SD of the Simpson-Index is seen, when dividing two groups by the median. (C) shows the *z*-scaled values (left) and the ranges of those *z*-scaled values (middle) of the single pixel-level parameters Simpson-Index (256 and 50) and Shannon-Index (256 and 50) as well SD od the Simpson-Index (265, right) for every patient. In (D), the different methylation classes for all biopsy every biopsy of all patients is depicted. As can be seen, in half of the cases, the classifier results of the different biopsies of one tumor showed diverging methylation classes. (E) shows a clear separation when separating groups by the number of different methylation classes in one tumor. Tumors with three different classes and therefore, epigenetically the most heterogenous tumors, show the poorest survival. Patients with tumors with non-diverging methylation classes lived the longest. In (F), the homogenous or heterogenous character for all four levels for every patient is given. In the upper row, the total heterogeneity score integrating all four levels can be seen. Part figure (G) shows the Kaplan-Meier curve for the separation by the mean *ProLoS*. Patients with a *ProLoS* above the mean survived significantly longer.

TABLE 3 Correlation of tumor size and biopsy distances with degree of heterogeneity.

Parameter		Modality I (*HisScore*)	Modality II (*NucDivScore*)	Modality III (SD of Simpson score)	Modality IV (*Entity ratio*)	All modalities (*UniPreHet-Ratio*)
Volume of CET	*r*	.092	.316	.088	.118	.287
	P	.598	.064	.615	.522	.094
Mean distance	*r*	**.363**	−.083	.012	**.413**	.331
	P	**.038**	.648	.947	**.019**	.060
Median distance	*r*	**.368**	−.043	.058	.332	.296
	P	**.035**	.813	.751	.064	.095

Note: Bold values indicate significant correlations.

data for 33 patients. Tumor size was determined as contrast enhancing tumor (CET) in MRI. No significant correlations were found when comparing tumor size and the degree of heterogeneity in all four modalities (represented by *HisScore*, *NicDivScore*, SD of Simpson Diversity Index and *Entity Ratio*) and a combined value represented by the *UniPreHet-Ratio* (Table 3). As could be expected, there was a significant correlation between the mean distances of the biopsies of the same patient and the *HisScore* ($r = .636$, $P = .038$), as well the *Entity ratio* ($r = .413$, $P = .019$; Table 3). There was also an association between the distances and the integrating *UniPreHet-Ratio*, although not significant ($r = .331$, $P = .060$).

4 | DISCUSSION

Intratumor heterogeneity is a hallmark of GBM but remains difficult to quantify. Moreover, morphological studies have mostly focused on one level of heterogeneity, usually by assessing regional heterogeneity by immunohistochemistry in samples of resected GBM.[6,7,24,25] For our study, 157 biopsies of 37 patients with therapy-naive IDH-wildtype GBM were analyzed. By separate examination of the single biopsies, an excellent spatial separation of different tumor areas is warranted. Besides traditional morphological analysis, we included novel scoring systems reflecting morphological intratumor heterogeneity and incorporated a new modality for heterogeneity by analyzing the pixel intensities in the GBM biopsies.

We were able to confirm our hypothesis that heterogeneity exists in different modalities. We observed a significant correlation between the distances of the biopsies to each other and the degree of heterogeneity on the regional and the epigenetic level, which seems biologically plausible and supports the validity of our analyses. Most interestingly, we can show an association between all modalities and OS. This led us to design a predictor of longer survival (*ProLoS*), which includes the four examined modalities of heterogeneity (regional, nuclear, pixel-level and epigenomic). By splitting the tumors into two groups with the mean *ProLoS* as cut-off, a highly significant separation regarding the OS was seen which underlines the clinical relevance of heterogeneity studies. When considering the single modalities, interestingly, the pixel-level showed inverted results compared to the other three levels. Whereas the comprehensive scores *HisScore* for the regional level, the *NucDivScore* for the cellular and the *entity ratio* for the epigenomic level all showed the trend that patients with heterogenous tumors have a shorter OS compared to tumors with lesser degree of heterogeneity, it was the other way around for the SD of the Simpson and Shannon Diversity Index. Both indices are usually used in ecology to describe biological diversity[26,27] and reflect the heterogeneity of pixel intensities in our study. This is an interesting finding contradicting the results one would expect. When reflecting the results, it makes sense, though, considering the fact that a high SD of the Simpson Diversity Index is equivalent with a high range of content of image information. A high range of information content could mean that the tumor features various morphological aspects differ regarding their information content. For instance, a tumor with biopsies that all include a high amount of necrosis would have, due to a high white content, generally low indices and hence, a low SD. To continue this thought, one would not expect that a GBM with globally high content of necrosis found in all biopsies has a better OS compared to a tumor that varies regarding its content of necrosis in the single biopsies. In general, GBM have an extremely high image information density in higher resolutions. This is why we decided to use SD as "zooming out" effect to capture differences at all.

For all other modalities, it was shown that higher degree of heterogeneity is associated with poorer survival, which is in line with previous studies.[7,10] It has to be noted, though, that some of these correlations are not significant, and their relevance has to be examined in further studies. Under the assumption that morphological heterogeneity is caused by genetic instability with the result of mutation accumulation, natural selection is a feasible explanation for tumor cell survival despite extensive therapy.[28] Individual therapies that are directed against specific genomic alterations, for instance, lose effectiveness when only a subpopulation is attacked due to clonal variation. The most significant result was seen for the epigenomic level. We were able to confirm our hypothesis that different GBM subtypes can be found in one single tumor. Moreover, we showed that patients with tumors that comprise three different methylation classes as defined by Capper et al[13] had a highly significantly shorter OS compared to patients with tumors that consisted of only one detected methylation class. Additionally to this interesting finding, it highlights the limitation of comprehensive epigenomic diagnostics based on a single biopsy. It also explains why therapies that are meant to treat specific genomic alterations have not shown the expected positive results in clinical practice. It should also be noted that we did not

analyze the whole tumor but a varying number of small biopsies. The assumption that all GBM show different subtypes to a certain degree seems likely. This entails the question how much tissue needs to be examined before a dimension of heterogeneity can be stated. Contrary to our results, Verburg et al stated that classification based on methylations profiles is highly conserved in space when the samples were adjusted for tumor purity.[29] This statement is also based on a study comprising spatially separated biopsies. Restrictively, the cohort included beside 7 IDH-wildtype GBM 9 IDH-mutant gliomas. As heterogeneity is generally more pronounced in IDH-wildtype, we assess our cohort of 37 patients with IDH-wildtype tumors more convincing. But indeed, the strongly debated issue of the influence of included non-neoplastic cells makes the matter even more difficult. We observed a highly positive correlation between the mesenchymal GBM subtype and the amount of Iba1-positive microglia. Even if this is in line with previous studies,[7,30,31] it raises the question how the amount of microglial cells and other non-neoplastic cells influences epigenetic and genetic analyses despite corrections for tumor purity. Our results show a significant inverse correlation between Iba1-positive cells and proliferating Mib1-positive cells. This is an expected result which validates our evaluation methods as one would anticipate that microglial cells do not proliferate as much as tumor cells.

A main limitation of our study is the selection bias. For the analyses, only tumor with at least three biopsies were included. Moreover, for further analyses that included epigenomic data, tumors with less than three biopsies with GBM methylation classes were excluded. Samples with classifier results of non-GBM-methylation classes were eliminated to avoid false results due to sampling error or low DNA quality. Furthermore, we correlated the degree of heterogeneity with the biopsy distances, although distance measurements can be inaccurate due to, for example, shifting during opening of the dura. Another shortcoming is that several histological parameters were manually scored, which might impede reproducibility. On the other hand, it avoids interobserver variance in the present study, as previously described.[32-34] While the manual selection of the snapshots introduces selection bias (toward images with high cell count), it also ensures a high quality of the image dataset. Due to the visual control, artifacts or regions with low or no tumor content were excluded, resulting in an easy to process dataset. Compared to the study by Andor et al,[16] in which ~15% of images had to be excluded from the analysis, this purity may actually prove as advantage.

Despite the limitations, we are convinced that our study gives a further confirmation that intratumor heterogeneity exists in GBM and has an impact on OS. By designing a predictor of longer survival, a way of possible clinical implementation of heterogeneity analysis is prepared. Certainly, such heterogeneity assessment needs thorough validation and simplification before it can be broadly applied. Furthermore, arising technologies including spatial proteomics/transcriptomics and multiplex immunohistochemistry should be complemented to validate the results and give further insights into the heterogenous constitution of GBM.

5 | CONCLUSION

Multiscale intratumor heterogeneity exists in glioblastoma and its degree has an impact on overall survival. In future studies, the creation and implementation of a broadly feasible heterogeneity index should be considered.

AUTHOR CONTRIBUTIONS

Georg Prokop: Conceived and designed our study; Analyzed the histological data; Did statistical analyses; Interpreted the data; Drafted the article and did the visualization. **Benedikt Wiestler:** Supervised the study; Made data available; Responsible for patient acquisition and biopsy planning; Did statistical analyses; Interpreted the data; Edited the article. **Daniel Hieber:** Did statistical analyses; Interpreted the data. **Fynn Withake:** Did statistical analyses; Edited the article. **Karoline Mayer:** Analyzed the histological data; Edited the article. **Jens Gempt:** Made data available; Responsible for patient acquisition and biopsy planning; Interpreted the data; Edited the article. **Claire Delbridge:** Made data available; Edited the article. **Friederike Schmidt-Graf:** Made data available; Did statistical analyses; Edited the article. **Nicole Pfarr:** Made data available; Edited the article. **Bruno Märkl:** Supervised the study; Edited the article. **Jürgen Schlegel:** Supervised the study; Made data available; Interpreted the data; Edited the article. **Friederike Liesche-Starnecker:** Conceived and designed our study; Analyzed the histological data; Interpreted the data; Drafted the article and did the visualization. The work reported in the article has been performed by the authors, unless clearly specified in the text. All authors approved to the final version of the article.

ACKNOWLEDGEMENTS

We would like to thank S. Baur and T. Matt for their excellent technical support. Open Access funding enabled and organized by Projekt DEAL.

FUNDING INFORMATION

Our study was supported by the Bavarian Cancer Research Center (BZKF; grant to F. Liesche-Starnecker; grant number ZB-003-2022) and the Deutsche Forschungsgemeinschaft (DFG; grant to B. Wiestler; SFB 824, subproject B12).

CONFLICT OF INTEREST STATEMENT

Nicola Pfarr declares that she has a potential financial conflict of interest as she has a participation in the advisory boards of Novartis, Bayer, Lilly, Roche and AstraZeneca, has received speaker fees from Illumina, Thermo Fisher Scientific, Roche, BMS, AstraZeneca, Bayer; MSD and QuiP; and traveling support from BMS, Illumina, Thermo Fisher Scientific and PGDx. All other authors declare that they have no conflict of interest.

DATA AVAILABILITY STATEMENT

The datasets generated and/or analyzed during the current study are available from the corresponding author on reasonable request.

ETHICS STATEMENT

Our study was approved by our local ethics committee (Technical University of Munich; 284/16S and 164/19S) and performed in accordance with the 1964 Helsinki declaration and its later amendments. All local patients were part of a prospective GBM cohort from February 2018 to March 2021 and gave written informed consent.

ORCID

Friederike Liesche-Starnecker https://orcid.org/0000-0003-1948-1580

REFERENCES

1. Aum DJ, Kim DH, Beaumont TL, Leuthardt EC, Dunn GP, Kim AH. Molecular and cellular heterogeneity: the hallmark of glioblastoma. *Neurosurg Focus*. 2014;37:E11.
2. Lee JK, Wang J, Sa JK, et al. Spatiotemporal genomic architecture informs precision oncology in glioblastoma. *Nat Genet*. 2017;49:594-599.
3. Verhaak RG, Hoadley KA, Purdom E, et al. Integrated genomic analysis identifies clinically relevant subtypes of glioblastoma characterized by abnormalities in PDGFRA, IDH1, EGFR, and NF1. *Cancer Cell*. 2010;17:98-110.
4. Parker NR, Hudson AL, Khong P, et al. Intratumoral heterogeneity identified at the epigenetic, genetic and transcriptional level in glioblastoma. *Sci Rep*. 2016;6:22477.
5. Koncar RF, Agnihotri S. Anarchy or respect the hierarchy? The complexity of glioblastoma. *Cancer Res*. 2020;80:3195-3196.
6. Bergmann N, Delbridge C, Gempt J, et al. The intratumoral heterogeneity reflects the intertumoral subtypes of glioblastoma multiforme: a regional immunohistochemistry analysis. *Front Oncol*. 2020;10:494.
7. Liesche-Starnecker F, Mayer K, Kofler F, et al. Immunohistochemically characterized Intratumoral heterogeneity is a prognostic marker in human glioblastoma. *Cancers (Basel)*. 2020;12:2964.
8. Lopes MB, Vinga S. Tracking intratumoral heterogeneity in glioblastoma via regularized classification of single-cell RNA-Seq data. *BMC Bioinform*. 2020;21:59.
9. Wenger A, Ferreyra Vega S, Kling T, Bontell TO, Jakola AS, Caren H. Intratumor DNA methylation heterogeneity in glioblastoma: implications for DNA methylation-based classification. *Neuro Oncol*. 2019;21:616-627.
10. Gempt J, Withake F, Aftahy AK, et al. Methylation subgroup and molecular heterogeneity is a hallmark of glioblastoma: implications for biopsy targeting, classification and therapy. *ESMO Open*. 2022;7:100566.
11. Sottoriva A, Spiteri I, Piccirillo SG, et al. Intratumor heterogeneity in human glioblastoma reflects cancer evolutionary dynamics. *Proc Natl Acad Sci U S A*. 2013;110:4009-4014.
12. Carpenter AE, Jones TR, Lamprecht MR, et al. CellProfiler: image analysis software for identifying and quantifying cell phenotypes. *Genome Biol*. 2006;7:R100.
13. Capper D, Stichel D, Sahm F, et al. Practical implementation of DNA methylation and copy-number-based CNS tumor diagnostics: the Heidelberg experience. *Acta Neuropathol*. 2018;136:181-210.
14. Louis DN, Perry A, Wesseling P, et al. The 2021 WHO classification of tumors of the central nervous system: a summary. *Neuro Oncol*. 2021;23:1231-1251.
15. Remmele W, Stegner HE. Recommendation for uniform definition of an immunoreactive score (IRS) for immunohistochemical estrogen receptor detection (ER-ICA) in breast cancer tissue. *Pathologe*. 1987;8:138-140.
16. Andor N, Graham TA, Jansen M, et al. Pan-cancer analysis of the extent and consequences of intratumor heterogeneity. *Nat Med*. 2016;22:105-113.
17. Caicedo JC, Cooper S, Heigwer F, et al. Data-analysis strategies for image-based cell profiling. *Nat Methods*. 2017;14:849-863.
18. Shannon CE. A mathematical theory of communication. *Bell Syst Tech J*. 1948;27:379-423.
19. Simpson EH. Measurement of diversity. *Nature*. 1949;163:688.
20. Reinhardt A, Stichel D, Schrimpf D, et al. Anaplastic astrocytoma with piloid features, a novel molecular class of IDH wildtype glioma with recurrent MAPK pathway, CDKN2A/B and ATRX alterations. *Acta Neuropathol*. 2018;136:273-291.
21. Capper D, Jones DTW, Sill M, et al. DNA methylation-based classification of central nervous system tumours. *Nature*. 2018;555:469-474.
22. Therneau TM, Grambsch PM. *G: Modelling Survival Data: Extending the Cox Model*. New York: Springer; 2000.
23. van der Maaten LJP, Hinton GE. Visualizing high-dimensional data using t-SNE. *J Mach Learn Res*. 2008;9:2579-2605.
24. Conroy S, Kruyt FA, Joseph JV, et al. Subclassification of newly diagnosed glioblastomas through an immunohistochemical approach. *PloS One*. 2014;9:e115687.
25. Popova SN, Bergqvist M, Dimberg A, et al. Subtyping of gliomas of various WHO grades by the application of immunohistochemistry. *Histopathology*. 2014;64:365-379.
26. Anderson K, Bennie J, Wetherelt A. Laser scanning of fine scale pattern along a hydrological gradient in a peatland ecosystem. *Landsc Ecol*. 2010;25:477-492.
27. Buckland ST, Magurran AE, Green RE, Fewster RM. Monitoring change in biodiversity through composite indices. *Philos Trans R Soc Lond B Biol Sci*. 2005;360:243-254.
28. Nowell PC. The clonal evolution of tumor cell populations. *Science*. 1976;194:23-28.
29. Verburg N, Barthel FP, Anderson KJ, et al. Spatial concordance of DNA methylation classification in diffuse glioma. *Neuro Oncol*. 2021;23:2054-2065.
30. Wang Q, Hu B, Hu X, et al. Tumor evolution of glioma-intrinsic gene expression subtypes associates with immunological changes in the microenvironment. *Cancer Cell*. 2018;33:152.
31. Lee SY, Zhu J, Salzberg AC, et al. Analysis of single nucleotide variants of HFE gene and association to survival in the cancer genome atlas GBM data. *PloS One*. 2017;12:e0174778.
32. Liesche-Starnecker F, Prokop G, Yakushev I, et al. Visualizing cellularity and angiogenesis in newly-diagnosed glioblastoma with diffusion and perfusion MRI and FET-PET imaging. *EJNMMI Res*. 2021;11:72.
33. Schon S, Cabello J, Liesche-Starnecker F, et al. Imaging glioma biology: spatial comparison of amino acid PET, amide proton transfer, and perfusion-weighted MRI in newly diagnosed gliomas. *Eur J Nucl Med Mol Imaging*. 2020;47:1468-1475.
34. Liesche F, Lukas M, Preibisch C, et al. (18)F-Fluoroethyl-tyrosine uptake is correlated with amino acid transport and neovascularization in treatment-naive glioblastomas. *Eur J Nucl Med Mol Imaging*. 2019;46:2163-2168.

SUPPORTING INFORMATION

Additional supporting information can be found online in the Supporting Information section at the end of this article.

How to cite this article: Prokop G, Wiestler B, Hieber D, et al. Multiscale quantification of morphological heterogeneity with creation of a predictor of longer survival in glioblastoma. *Int J Cancer*. 2023;153(9):1658-1670. doi:10.1002/ijc.34665